Supplementary Information: Narrow magneto-optical transitions in Erbium implanted silicon carbide-on-insulator

Alexey Lyasota[1†], Joshua Bader[2,3†], Shao Qi Lim[4], Brett C. Johnson[5], Jeffrey C. McCallum[4], Qing Li[6], Sven Rogge[1*], Stefania Castelletto[2*]

[1]Centre of Excellence for Quantum Computation and Communication Technology, School of Physics, University of New South Wales, Sydney, NSW 2052, Australia.
[2]School of Engineering, RMIT University, Melbourne, 3000, VIC, Australia.
[3]Centre for Quantum Computation and Communication Technology, School of Engineering, RMIT University, Melbourne, 3000, VIC, Australia.
[4]Centre for Quantum Computation and Communication Technology, School of Physics, The University of Melbourne, Melbourne, 3010, VIC, Australia.
[5]School of Science, RMIT University, Melbourne, 3001, VIC, Australia..
[6]Electrical and Computer Engineering, Carnegie Mellon University, Pittsburgh, 15213, PA, USA.

*Corresponding author(s). E-mail(s): s.rogge@unsw.edu.au; stefania.castelletto@rmit.edu.au;
Contributing authors: a.lyasota@unsw.edu.au;
†These authors contributed equally to this work.

Contents

Introduction

In this Supplementary Information, we show additional data supporting our conclusions given in the main text. In Section I, we present detailed identification of all lines in the photoluminescence excitation spectrum and provide the fits for inhomogeneous photoluminescence excitation (PLE) lines of sites α and β. Section II shows photoluminescence (PL) spectra that allow us to unambiguously identify sites α and β. Section III focuses on a detailed energy level diagram of all observed Er-sites, while section IV shows the identification of lines with long optical coherence based on measurements performed with broadband and narrow linewidth excitations.

Section I. Observed photoluminescence excitation lines

Fig. S1 shows PLE spectra of the 19 peaks identified in the PLE spectrum shown in the main text.

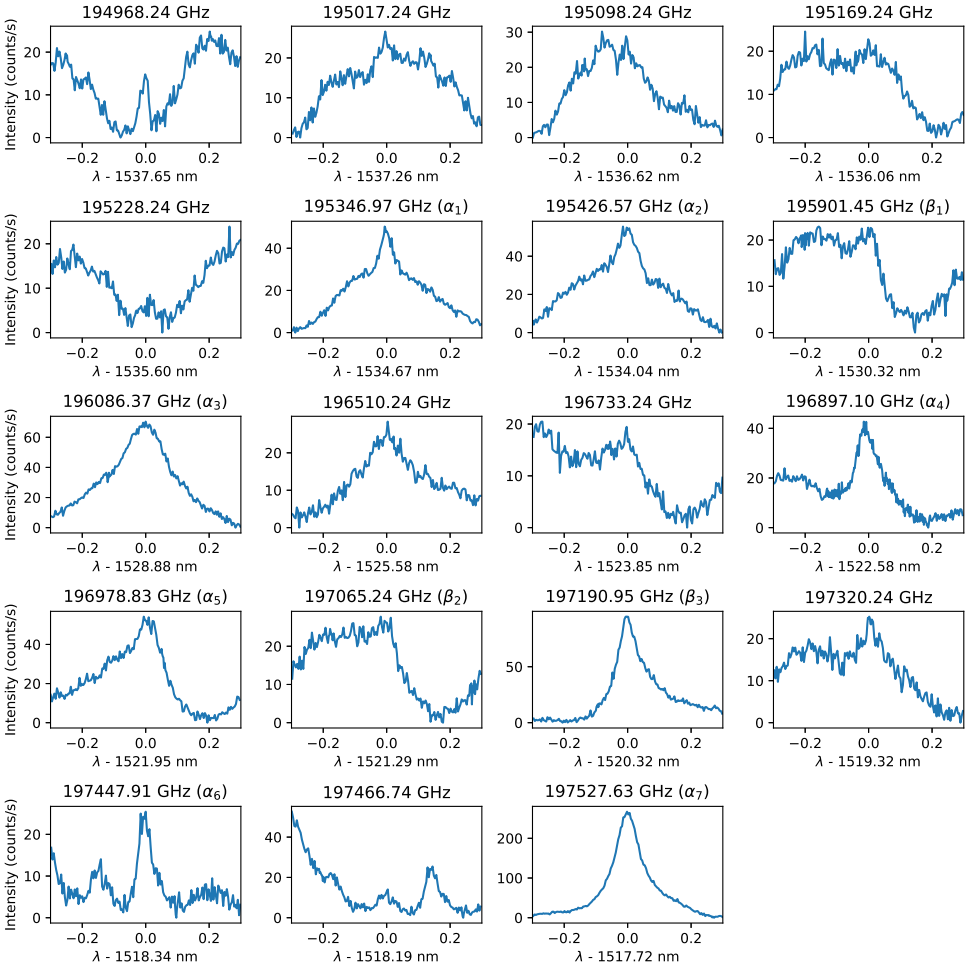

Fig. S1 Observed optical transitions in PLE spectrum. The center frequency for every line is given in the corresponding panel's title. The centre frequencies for sites α and β are obtained for Gaussian fits given below. The excitation pulse and measurement interval were 20 μs and 170 μs.

The identified PLE peaks of α and β sites were fitted using the Gaussian profile (see Fig.S2 and Fig.S3). To obtain clear Gaussian fits, the Fabry-Pérot-related modulation of the PLE spectrum was accounted for using a linear approximation for the slope under the PLE lines (see Fig.S2 and Fig.S3).

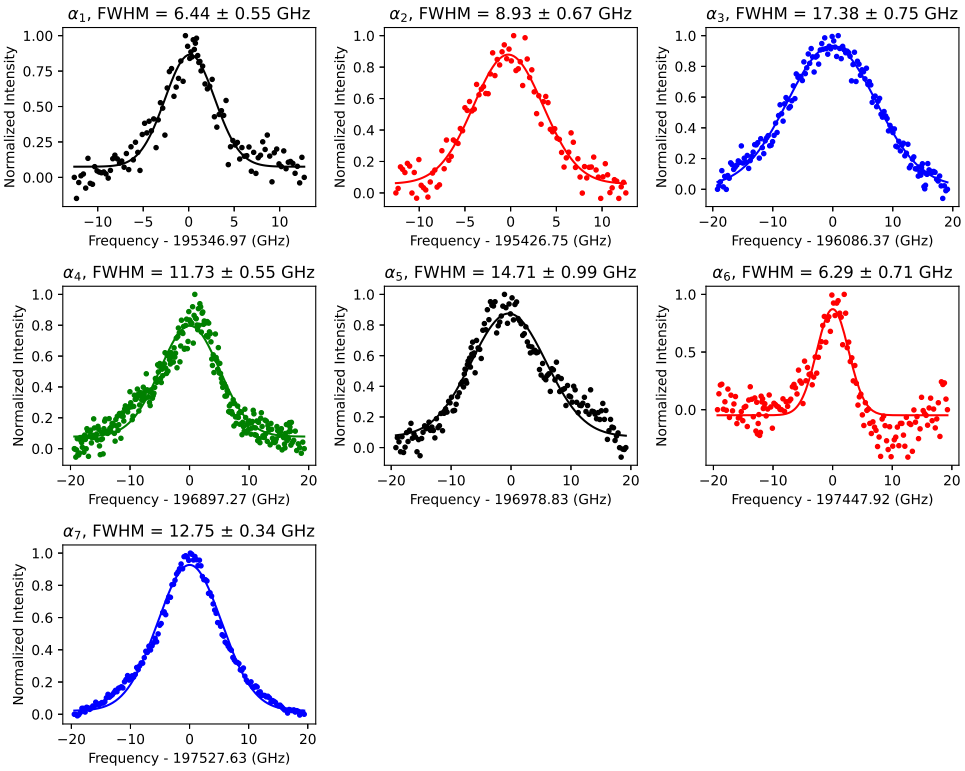

Fig. S2 Gaussian fits of the site α PLE resonances. The FWHM uncertainty is estimated as the 95% confidence interval. These resonances were obtained from S1 by subtracting the sloped background using a linear fit.

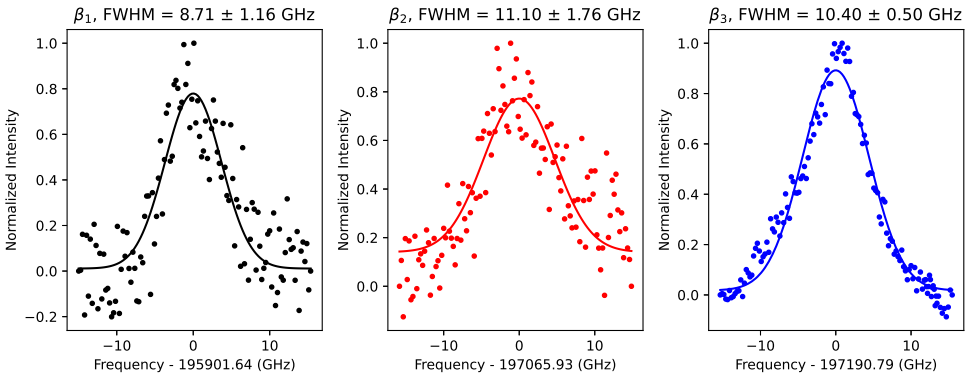

Fig. S3 Gaussian fits of the site β PLE resonances. The FWHM uncertainty is estimated as the 95% confidence interval. These resonances were obtained from S1 by subtracting the sloped background using a linear fit.

Section II. Identification of Er sites

Fig. S4 shows photoluminescence (PL) spectra measured using the tunable optical filter (TOF) for the brightest lines in the PLE spectrum. Most of the PL spectra yielded clear PL peaks. The correlations between the PL and PLE peak locations allowed us to identify sites' α and β ressonaces. It should be noted that we observed an increase in the signal when the laser and TOF optical frequencies were the same. This resulted in spurious lines appearing in the PL spectra at the excitation frequency (see for example the PL spectrum excited via the α_3 transition in Fig. S4, second panel from the top).

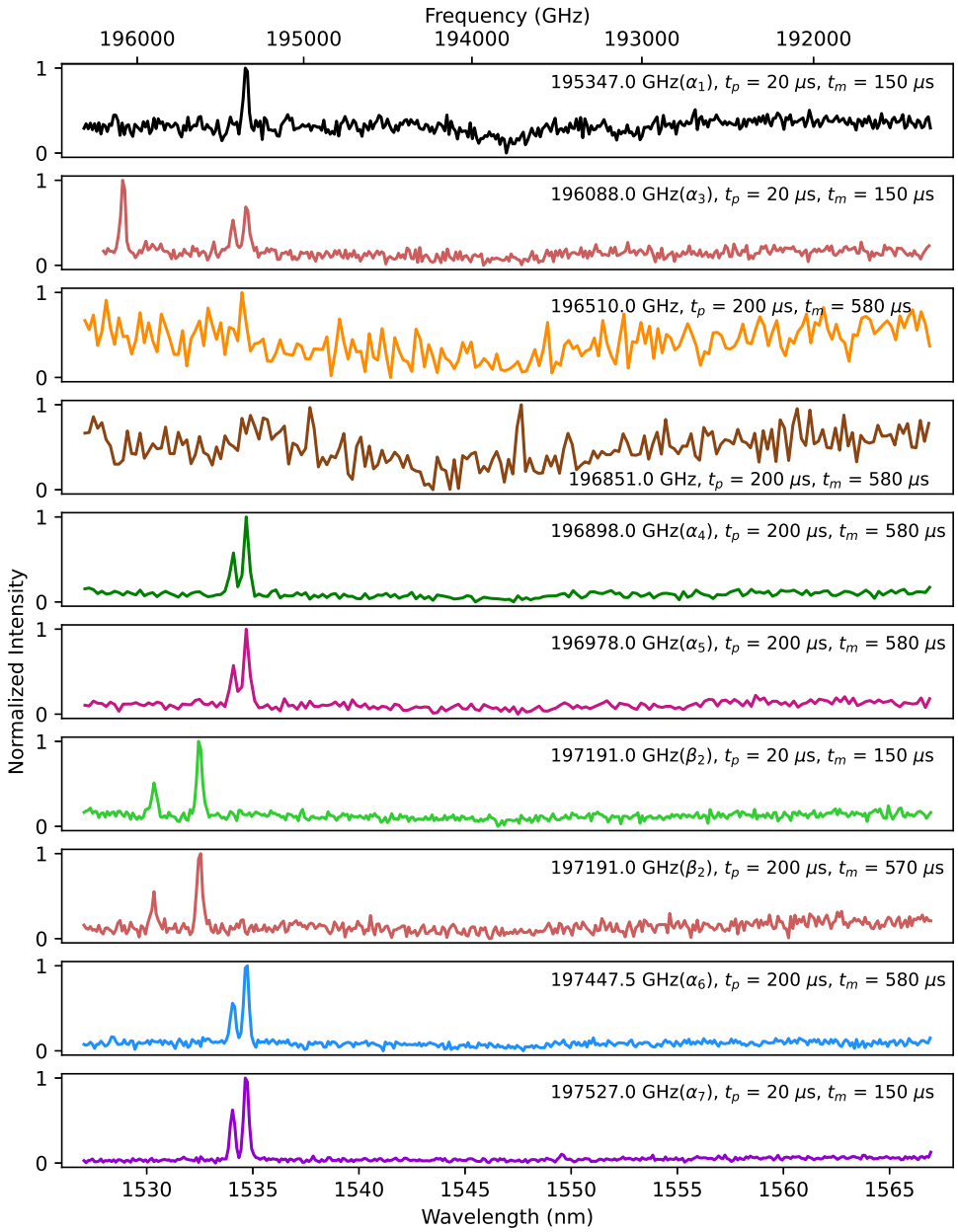

Fig. S4 PL spectra resonantly excited via the brightest PLE lines. The excitation laser frequency, the assigned site, the excitation pulse width t_p, and the measurement interval t_m are given in each panel. The PL scanning range was limited by the TOF range of 1527 to 1567 nm. The third (orange) and fourth (brown) PL-spectra are obtained by driving a PLE-line which cannot be associated with any site.

We did additional correlation PL measurements to ensure that the low intensity α and β PLE transitions are properly assigned. The TOF was tuned within the narrow 0.65 nm spectral range accross α_1 (Fig. S5) and β_{PL1} (Fig. S6) lines while the laser was consecutively centered at the nonidentified PLE lines.

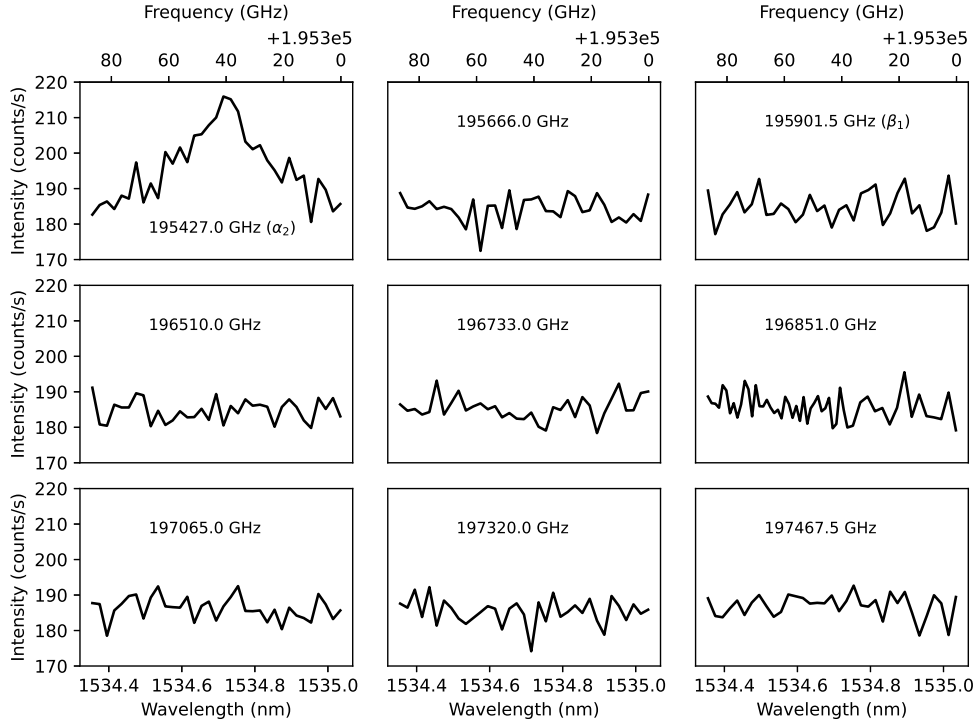

Fig. S5 PL spectra measured near the α_1 transition. The excitation was conducted at the identified PLE lines with the frequencies higher than the α_1 transition frequency excluding transitions for which the full PL spectra were measured (Fig. S4). The excitation laser frequency is given in each panel. The peak visible at the 195427 GHz when excited at the α_2 PLE transition frequency corresponds to the emission at the α_1 transition frequency. The excitation pulse and measurement interval were 20 μs and 140 μs.

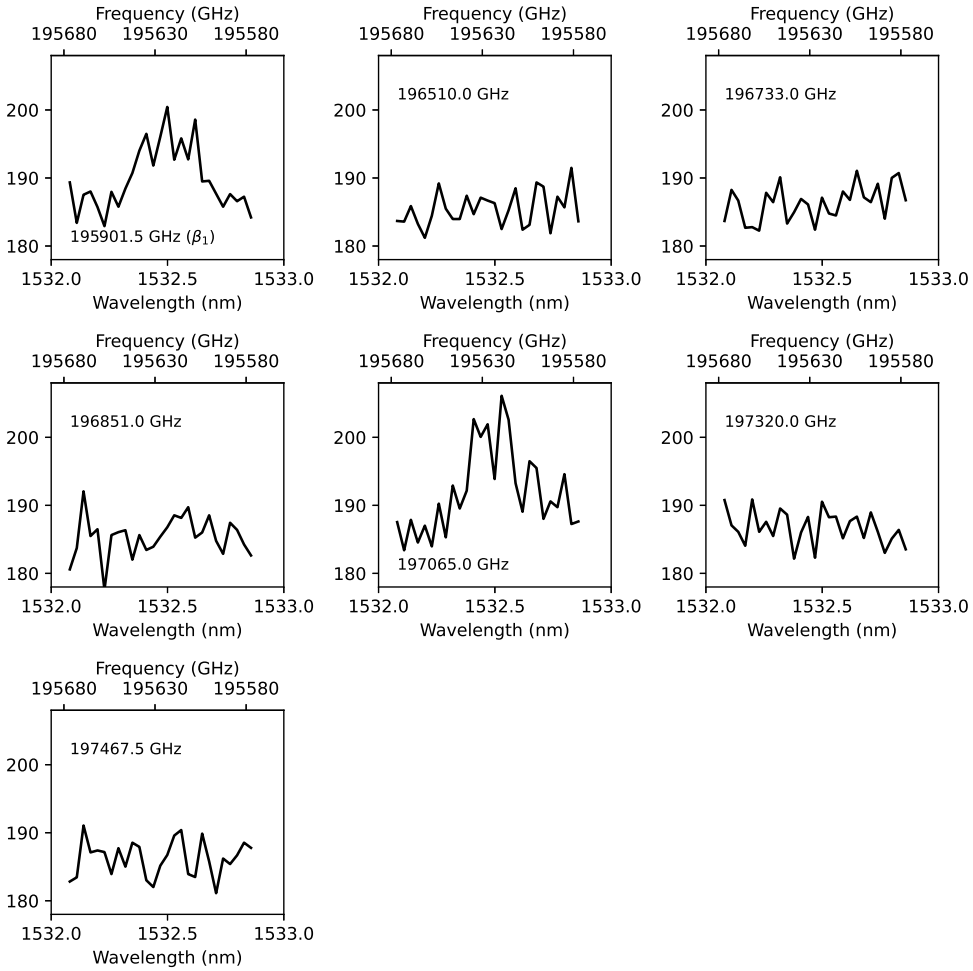

Fig. S6 PL spectra measured near the lowest energy PL transition of the β_{PL1} site by tuning the TOF wavelength across β_{PL1} center frequency. The excitation was conducted at the identified PLE lines with the frequencies higher than the β_{PL1} PL transition frequency for which the full PL spectra were not measured (see Fig. S4). The excitation laser frequency is given in each panel. The PL signal obtained at the 195901.5 corresponds to the β_1 PLE transition. The PL signal obtained at the 197065.0 GHz excitation frequency allows assigning this PLE transition to the β_2 line (the second highest energy PLE line of the site β. The excitation pulse and measurement interval were 20 μs and 140 μs.

We verified that neither of the identified PLE lines corresponds to the l_1 PLE line observed at 194969 GHz (see Fig. S7). The TOF filter was scanned across the l_1 line in a similar manner as above while the laser was centered at all non identified lines as well as several α and β PLE lines.

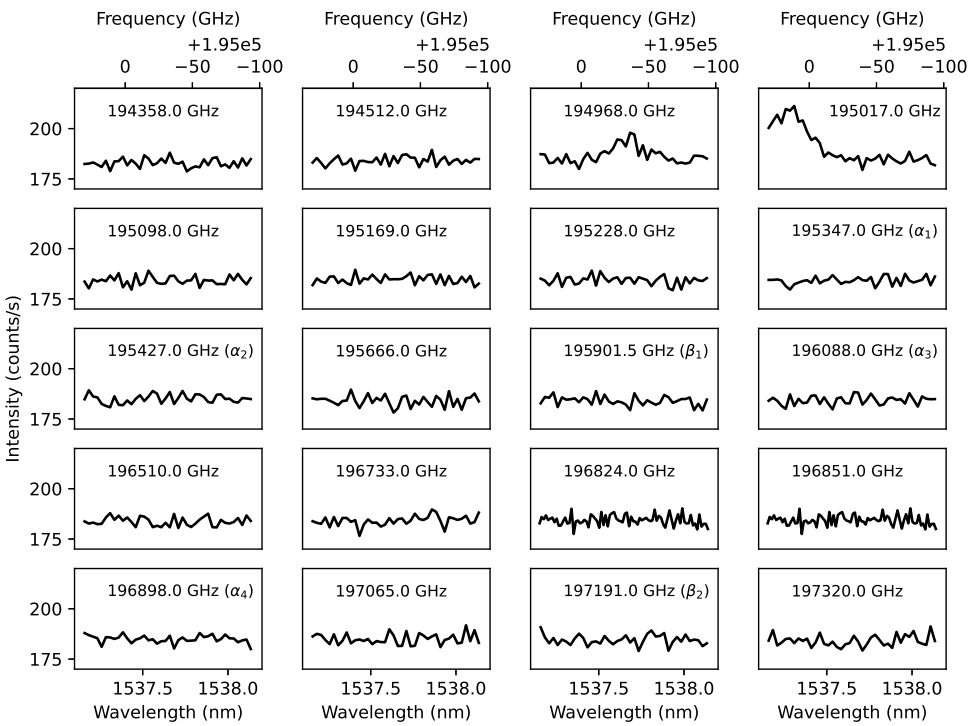

Fig. S7 PL spectra measured near the l_1 transition observed at 194969 GHz. The excitation was conducted at all nonidentified PLE lines and several α and β PLE transitions. The excitation laser frequency is given in each panel. Peaks visible at the excitation frequencies 194968 and 195017 GHz are due to the spurious signal at the laser excitation frequencies. The excitation pulse and measurement interval were 20 μs and 140 μs.

Section III. Energy level diagram from the identified Er sites

The information presented in the main section about the crystal field splitting is summarized here in Fig. S8. A detailed summary of the exhibited center frequency differences (α_{i-1} and β_{i-1}) and their subsequent wavenumber is shown in Fig. S8**a**. For this, each specific resonance i (α_i and β_i) is normalized to the highest energy transition (either α_1 or β_1) of each individual site (α and β). This is further illustrated in Fig. S8**b** showing the observed crystal fields within a diagram levels. The separation between each individual $^4I_{13/2}$ excited state crystal field is identified as the individual center frequency difference. $\alpha_{3,\ldots,7}$ resonances originate either from the lowest or second-lowest $^4I_{15/2}$ crystal field while $\alpha_{1,2}$ exhibit properties to relax to the same $^4I_{15/2}$ ground state crystal field but emerge from distinct low-lying excited state fields. $\beta_{1,2,3}$ are implemented according to their wavenumber.

a

Site α

	Freq. Difference (GHz)	Wavenumber (cm^{-1})
α_1	195347.0	6516.07
$\alpha_{2\text{-}1}$	79.6	2.66
$\alpha_{3\text{-}1}$	739.4	24.66
$\alpha_{4\text{-}1}$	1550.1	51.71
$\alpha_{5\text{-}1}$	1631.9	54.43
$\alpha_{6\text{-}1}$	2100.9	70.08
$\alpha_{7\text{-}1}$	2180.6	72.74
	Site β	
β_1	195901.4	6534.58
$\beta_{2\text{-}1}$	1164.5	38.8
$\beta_{3\text{-}1}$	1289.3	43.0

b

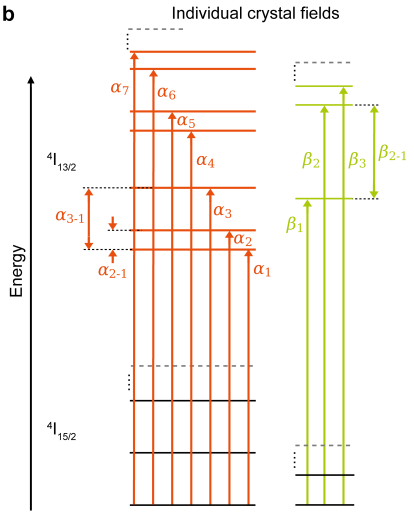

Fig. S8 Detailed energy levels structure from the observed Er^{3+} sites in 4H-SiCOI: **a** table summarizing the resonance frequencies of all observed transitions of sites α and β between the $^4I_{15/2}$ lowest energy level and the $^4I_{13/2}$ manifold. The values shown here are quoted relative to the lowest $^4I_{13/2}$ energy level, α_1 and β_1, in units of frequency and wavenumber; **b** schematic energy level diagram detailing distinct energy level separations via the observed frequency difference between specific resonances within the $^4I_{13/2}$ excited state manifold.

Section IV. Identification of optical transitions with long optical coherence time

We identified PLE resonances with narrow homogeneous linewidth by performing excitation with 'monochromatic' ($<$ 100 kHz) and 'broad' (60 MHz) excitation linewidths. The 'narrow' linewidth corresponds to the PurePhotonics PPCL550 laser expected to be well below 100 kHz (10 kHz instantaneous linewidth) obtained by integrating the linewidth over the 20 μm excitation pulse. The 60 MHz broad excitation was achieved by broadening the laser linewidth using an electro-optical modulator (EOM) whicch resulted in a 60 MHz top-hat excitation spectrum. The 'narrow' and 'broad' excitation resulted in significant difference in the PLE intensity if the homogeneous linewidth γ_h was smaller than 60 MHz.

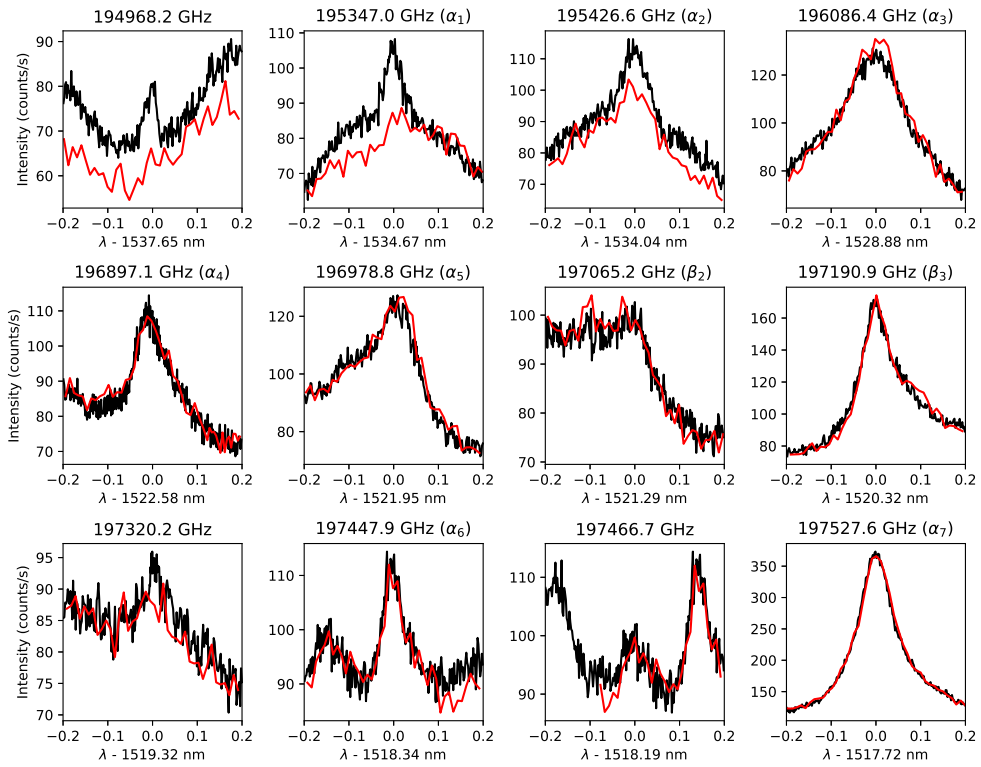

Fig. S9 PLE spectra measured using 60 MHz broad (black) and monochromatic (< 100 kHz) laser excitation (red). The excitation pulse and measurement interval were 20 μs and 170 μs. The large difference in obtained spectra indicate the narrow homogeneous linewidth. All observed resonances are individually shown with the unassigned resonance l_1 in the top left corner while assigned resonances α_i and β_i are specifically labeled.